

J. L. Mosenfelder

Pressure dependence of hydroxyl solubility in coesite

Received: 23 August 1999 / Accepted: 10 April 2000

Abstract The solubility of hydroxyl in coesite was investigated in multianvil experiments performed at 1200 °C over the nominal pressure range 5–10 GPa, at an f_{O_2} close to the Ni-NiO buffer. The starting material for each experiment was a cylinder of pure silica glass plus talc, which dehydrates at high P and T to provide a source of water and hydrogen (plus enstatite and excess SiO_2). Fourier-transform infrared (FTIR) spectra of the recovered coesite crystals show five sharp bands at 3606, 3573, 3523, 3459, and 3299 cm^{-1} , indicative of structurally bonded hydrogen (hydroxyl). The concentration of hydrogen increases with pressure from 285 H/10⁶ Si (at 5 GPa) to 1415 H/10⁶ Si (at 10 GPa). Assuming a model of incorporation by (4H)_{Si} defects, the data are fit well by the equation $C_{\text{OH}} = Af_{\text{H}_2\text{O}}^2 \exp(-P\Delta V/RT)$, with $A = 4.38 \text{ H}/10^6 \text{ Si/GPa}$, and $\Delta V = 20.6 \times 10^{-6} \text{ m}^3 \text{ mol}^{-1}$. An alternative model entailing association of hydrogen with cation substitution can also be used to fit the data. These results show that the solubility of hydroxyl in coesite is approximately an order of magnitude lower than in olivines and pyroxenes, but comparable to that in pyropic garnet. However, FTIR investigations on a variety of ultrahigh pressure metamorphic rocks have failed in all cases to detect the presence of water or hydrogen in coesite, indicating either that it grew in dry environments or lost its hydrogen during partial transformation to quartz. On the other hand, micro-FTIR investigations of quartz crystals replacing coesite show that they contain varying amounts of H_2O . These results support the hypothesis that preservation of coesite is not necessarily linked to

fast exhumation rates but is crucially dependent on limited fluid infiltration during exhumation.

Key words Coesite · Stishovite · Multianvil · OH solubility · Infrared spectroscopy

Introduction

It has long been known that quartz can dissolve small amounts of water into its structure as hydrogen defects (see Paterson 1989 for review). Recent work has shown that other “nominally anhydrous minerals” – such as olivines, pyroxenes, and garnets – can incorporate significantly greater amounts of hydrogen in their structures than quartz (e.g., Kohlstedt et al. 1996; Rossman 1996; Lu and Keppeler 1997). Interest in the effects of pressure on the solubility of water (as hydroxyl, OH) in these phases stems from the realization that they may provide a major reservoir for hydrogen in the Earth and facilitate recycling of water into the mantle to depths beyond the stability limit of hydrous phases (Bell and Rossman 1992; Rossman 1996). Furthermore, it is well known that trace amounts of hydrogen can drastically influence a wide variety of physical properties of rocks, including rheology, melting temperature, electrical conductivity, and diffusion kinetics. Incorporation of trace amounts of hydrogen in minerals can therefore have important consequences for large-scale chemical and dynamical processes in the crust and mantle.

The effect of increasing pressure on hydroxyl solubility in nominally anhydrous minerals has been systematically studied in olivine and its high-pressure polymorphs (Kohlstedt et al. 1996) and pyrope garnet (Lu and Keppeler 1997). Pawley et al. (1993) showed that stishovite, one of the high-pressure forms of SiO_2 , can incorporate significant amounts of hydrogen at 10 GPa (up to ~550 H/10⁶ Si), especially when coupled to Al substitution. Preliminary results were also reported by Li et al. (1997) at a single pressure (7 GPa) on coesite, another high-pressure form of SiO_2 stable at pressures interme-

J. L. Mosenfelder
Bayerisches Geoinstitut, Universität Bayreuth,
95440 Bayreuth, Germany

Present address:
Division of Geological and Planetary Sciences,
California Institute of Technology, M/C 170-25, Pasadena,
California 91125, USA
e-mail: jed@gps.caltech.edu

diate between quartz and stishovite. In this study I have measured the pressure dependence of hydroxyl solubility in pure coesite over a broad pressure range (5 to 10 GPa).

The discovery of coesite in regionally metamorphosed rocks (see Coleman and Wang 1995 for review) demonstrated that significant portions of continental crust have been subducted to depths >100 km and subsequently exhumed to the surface. One of the enduring problems related to ultrahigh-pressure (UHP) metamorphism concerns the timing and style of exhumation. Models for exhumation must account for the preservation of highly metastable phases such as coesite. The most commonly offered explanation is that phases surrounding coesite crystals act as "pressure vessels", inhibiting transformation by keeping a high pressure on the included coesite (Gillet et al. 1984). However, an equally important factor in the metastability of coesite might be the availability of hydrogen and/or H₂O, both of which can flux backreaction to quartz during exhumation. One motivation for the present study is to test the possibility that hydrogen incorporated in coesite crystals at high pressure and temperature influences the preservation of coesite in UHP rocks.

Experimental and analytical methods

High-pressure experiments

The starting material for all experiments consisted of a 2-mm diameter cylinder of Corning grade G silica glass (approximately 70–100 mg) plus 100–200 mg of synthetic talc, which dehydrates at high P and T to provide a source of water (plus enstatite and excess SiO₂). These materials were loaded into 2.2-mm-diameter Pt capsules, which were subsequently welded shut. In all experiments except one (no. S1686), a layer of Ni/NiO powder (mixed 1:1 by volume) was also added to one end of the capsule in order to buffer oxygen fugacity. According to the manufacturers' specifications, the glass contains <150 ppb of any contaminant with the exception of hydroxyl, measured at 2850 ± 40 H/10⁶ Si by Fourier-transform infrared (FTIR) spectroscopy (Mosenfelder and Bohlen 1997), and the talc is 99.99% pure. The purity of the Ni-NiO powder mixture is unknown, however, and trace amounts of elements such as Fe could have been introduced into the samples during preparation.

Experiments were conducted at 1200 °C and 5–10 GPa, using 6–8-type multianvil apparatus (Table 1). Five of the experiments were conducted in a 1000-tonne press, whereas one (no. S1686) was conducted in a 1200-tonne press. Pressure assemblies consisted of Cr-doped MgO octahedra with an edge length of 18 mm, containing stepped LaCrO₃ furnaces. Temperature was measured using coaxial W3%Re-W25%Re thermocouples. Details of the pressure

calibration are presented in Rubie et al. (1993). The pressure uncertainty is generally estimated to be ±0.5 GPa. However, under the conditions of the experiments, an exceptionally large volume reduction occurs as a result of crystallization of the low-density glass (2.2 g cm⁻³) to coesite (2.92 g cm⁻³) and stishovite (4.3 g cm⁻³). Consequently, a pressure drop may occur that is not compensated for by the system. This could explain the coexistence of both stishovite and coesite (see below) in run no. 1109, at a nominal pressure of 10 GPa, 0.8 GPa above the equilibrium boundary (Zhang et al. 1996). Note that coesite was also present at 10 GPa in the experiments of Pawley et al. (1993), who explained its presence as a metastable quench product. Evidence for similar pressure drops associated with solid–solid phase transformations has been discussed by Rubie (1999). Because of this problem, the nominal pressures of all the experiments may be systematically high and therefore both the precision and accuracy of pressure are difficult to assess. However, this uncertainty has no serious implications for the conclusions of the present work.

At the end of each experiment, temperature was quenched to less than 400 °C in 1–2 s by cutting power to the furnace, and then the pressure was decreased. The presence of excess water (as vapor) in all of the recovered samples was verified by filing a small hole in the end of the retrieved capsule. Thick (ca. 80–100 µm) and thin (30 µm) sections were then made for conducting FTIR spectroscopy, optical microscopy, and electron microprobe analysis. The sections were cut without regard to crystal orientation, as the samples were polycrystalline (Fig. 1). The thickness of the sections was measured by a digital micrometer and is considered accurate to ±3 µm.

FTIR spectroscopy

Infrared spectra on experimental and natural samples were acquired using a Bruker IFS 120 FTIR spectrometer coupled with a Bruker infrared microscope. Details of the instrument specifications can be found in Kohlstedt et al. (1996) and Lu and Keppler (1997). Spectra were recorded by averaging 200 or more scans with 1 cm⁻¹ resolution, using a tungsten light source and CaF₂ beam splitter. The samples were immersed in polytrichloroethylen oil, which is free of absorption bands in the 4000 to 3000 cm⁻¹ region, in order to reduce interference fringes. Analyses were conducted using an aperture of 20 to 100 µm, allowing selection of areas free of cracks and fluid inclusions. The spectra were corrected to eliminate high-frequency peaks due to traces of water in the beam, smoothed, and then corrected for nonlinear background using a spline fit of the baseline.

OH concentrations for most minerals were estimated by integrating the absorption of unpolarised spectra from 3700 to 3000 cm⁻¹, using the wavenumber-dependent, empirical calibration of Paterson (1982):

$$C_{\text{OH}} = \frac{B_i}{150\zeta} \int \frac{H(\nu)}{(3780 - \nu)} d\nu,$$

where C_{OH} is the molar concentration of hydroxyl, ζ is an orientation factor (1/3 for unpolarized measurements), $H(\nu)$ is the absorption coefficient in cm⁻¹ and ν is wavenumber in cm⁻¹. The uncertainty of these measurements is limited by two factors:

Table 1 Experimental conditions and results

Run no.	P (GPa)	$f_{\text{H}_2\text{O}}$ (GPa)	Time (h)	C_{OH} (H/10 ⁶ Si) ^a	$C_{\text{H}_2\text{O}}$ (wt ppm H ₂ O)	Mineral assemblage ^b
886	5	5.3×10^2	12	284 ± 38 (10)	43	Co, Px, Sp, NNO
887	6.5	2.8×10^3	12	566 ± 54 (5)	85	Co, Px, Sp, NNO
S1686	7	4.8×10^3	15	729 ± 61 (18)	109	Co, En
885	8	1.3×10^4	12	1219 ± 66 (11)	183	Co, Px, Sp, NNO
917	9	3.6×10^4	12	1261 ± 105 (11)	189	Co, Px, Sp, NNO
1109	10	7.7×10^4	12	1415 ± 73 (11)	212	Co, St, Px, Sp, NNO

^a Number in parentheses is the number of spot measurements used for calculation

^b Co Coesite, St stishovite, Px Ni-pyroxene, En enstatite, Sp (Ni,Mg)₂SiO₄-spinel, NNO Ni + NiO

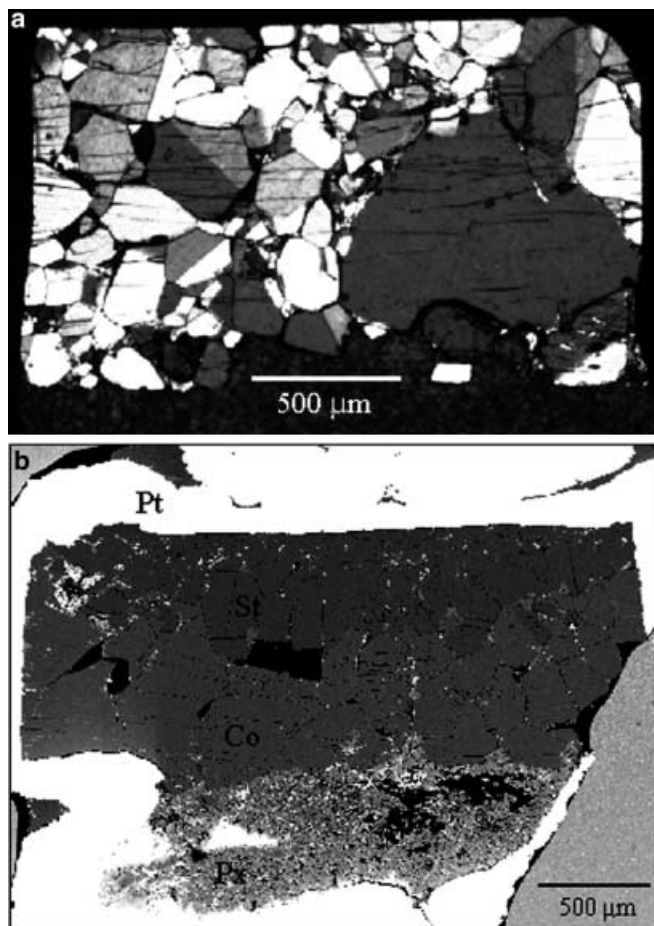


Fig. 1 **a** Optical photomicrograph (cross-polarized light) of sample no. 885 showing large coesite crystals. **b** Backscattered electron (BSE) image of sample no. 1109. Stishovite (*St* dark gray) crystallized at the top of the capsule, whereas coesite (*Co* lighter gray) formed in the middle (see text). The sharp BSE contrast between these two phases is surprising given the practically identical average atomic number of the phases. It is probably caused by the difference in the BSE coefficient associated with the large density contrast between coesite and stishovite (cf. Mosenfelder and Bohlen 1997). Also shown are the Pt capsule (*Pt*) and Ni-rich pyroxene (*Px*); *black areas* are where crystals were plucked out during polishing

the accuracy of the calibration, and the use of unpolarized radiation on randomly oriented crystals, which can lead to large errors if the orientation dependence of the OH-stretching frequencies is large (Rossman 1996). Although the accuracy of the empirical Paterson (1982) calibration is commonly estimated to be in the range of ± 30 to 50% (e.g., Kohlstedt et al. 1996), direct calibrations on some minerals (e.g., Bell et al. 1995) show much larger discrepancies. Unfortunately, direct experimental calibrations (e.g., by manometry) for the minerals analyzed in this study are not yet available. The effect of using unpolarized radiation was assessed by performing a number of measurements on crystals in different orientations, as discussed further below.

Electron microprobe

Chemical analyses were performed using a Cameca SX50 electron microprobe at Bayreuth and a JEOL 733 at Caltech, both operated at 15 kV accelerating potential and 15–20 nA beam current, with a spot size of 1 μm . Well-characterized natural and synthetic standards (including synthetic Ni-olivine) were used for calibration.

The estimated detection limit for minor elements under the operating conditions is 0.02 wt%. Some analyses of coesite gave low totals, presumably due to poor-quality sample polish. Unfortunately, all of the samples with the exception of no. 1109 were subsequently damaged and could not be reanalyzed.

Experimental results

Mineral assemblages and textures

Mineral assemblages in the recovered samples are listed in Table 1. All samples contain coesite crystals up to several hundred microns in diameter (Fig. 1). Stishovite crystals (up to 460 by 160 μm in size) were also found clustered together at one end of the capsule in sample no. 1109 (Fig. 1b). The spatial relationship between the two phases is consistent with initial nucleation and growth of stishovite at the edge of the glass cylinder, followed by a pressure drop and subsequent growth of coesite, as discussed above. Microprobe analyses (Table 2) indicate that some of the coesite and stishovite crystals contain small amounts of Al_2O_3 , TiO_2 , Cr_2O_3 , FeO, NiO, and K_2O , but the measurements are close to the detection level under the operating conditions of the analysis.

In addition to the silica phases, the samples contain fine-grained enstatite with varying Ni contents, small amounts of $(\text{Ni,Mg})_2\text{SiO}_4$, Ni metal, and NiO (Fig. 2). The $(\text{Ni,Mg})_2\text{SiO}_4$ phase probably has a spinel structure, which should be stable (as opposed to Ni-rich olivine) at the conditions of the experiments (Rubie et al. 1990). Similar reaction products were found in the study of Kohlstedt et al. (1996). The sample synthesized without the Ni-NiO buffer (no. S1686) contains only coesite and pure Mg-end member enstatite. Microprobe analyses revealed a wide range of Ni contents in the pyroxenes, from 0 to 15 wt%. Some Ni-rich pyroxenes are zoned, with Ni content increasing towards the rim (see Table 2). These observations indicate that Ni mobility in the grain boundary fluid was high but that chemical equilibrium was not achieved. $(\text{Ni,Mg})_2\text{SiO}_4$, when present, forms a well-defined rim between pyroxene and Ni-NiO, possibly representing a reaction between the excess silica derived from the breakdown of talc and the NiO. The Ni and NiO exhibit a eutectoid-like texture (Fig. 2), suggesting that oxygen fugacity could have been buffered by these phases and communicated along the interconnected grain boundaries between them to the rest of the capsule.

FTIR spectroscopy

Typical unpolarized FTIR spectra for the phases are shown in Fig. 3. Coesite displays four sharp peaks at 3573, 3523, 3459, and 3298 cm^{-1} (Fig. 3a). In some spectra, an additional, much smaller peak on the shoulder of the 3573 cm^{-1} band is observed at 3606 cm^{-1} . The locations of the three largest peaks are in good agreement with the assignments of Li et al. (1997). The sharpness of the peaks is interpreted to be an

Table 2 Selected microprobe analyses

Sample phase	1109 Coesite	1109 Coesite	1109 Coesite	1109 Coesite	917 Coesite	1686 Coesite	1109 Stishovite	1109 Stishovite	1109 Stishovite	1109 Ni-rich pyroxene Core	1109 Ni-rich pyroxene Rim	917 Ni-rich pyroxene	917 Ni-rich spinel ^a
SiO ₂	100.76	99.79	100.74	100.78	96.74	97.20	99.99	99.94	100.33	60.47	57.78	54.66	30.26
Al ₂ O ₃	0.00	0.00	0.00	0.01	0.01	0.01	0.09	0.03	0.03	0.07	0.04	0.08	0.03
TiO ₂	0.03	0.01	0.00	0.00	n.a.	n.a.	0.00	0.00	0.00	0.01	0.02	n.a.	n.a.
Cr ₂ O ₃	0.01	0.00	0.01	0.00	n.a.	n.a.	0.00	0.04	0.00	0.01	0.00	n.a.	n.a.
FeO	0.01	0.00	0.01	0.00	0.00	0.00	0.02	0.00	0.00	0.36	0.30	0.21	0.03
MgO	0.00	0.00	0.00	0.00	0.00	0.00	0.00	0.00	0.00	37.72	31.07	29.56	6.78
NiO	0.03	0.00	0.00	0.00	0.00	0.00	0.01	0.00	0.03	3.65	12.35	15.34	63.85
CaO	0.00	0.01	0.00	0.01	n.a.	n.a.	0.01	0.00	0.00	0.04	0.05	n.a.	n.a.
Na ₂ O	0.00	0.00	0.00	0.00	n.a.	n.a.	0.00	0.00	0.00	0.00	0.00	n.a.	n.a.
K ₂ O	0.02	0.01	0.01	0.02	n.a.	n.a.	0.01	0.02	0.02	0.02	0.02	n.a.	n.a.
Total	100.85	99.83	100.77	100.82	96.75	97.21	100.12	100.03	100.40	102.36	101.62	99.84	100.96
Si	1.000	1.000	1.000	1.000	1.000	1.000	0.999	0.999	1.000	2.009	2.013	1.975	0.992
Al	0.000	0.000	0.000	0.000	0.000	0.000	0.001	0.000	0.000	0.003	0.002	0.003	0.001
Ti	0.000	0.000	0.000	0.000	n.a.	n.a.	0.000	0.000	0.000	0.000	0.001	n.a.	n.a.
Cr	0.000	0.000	0.000	0.000	n.a.	n.a.	0.000	0.000	0.000	0.000	0.000	n.a.	n.a.
Fe	0.000	0.000	0.000	0.000	0.000	0.000	0.000	0.000	0.000	0.010	0.009	0.006	0.001
Mg	0.000	0.000	0.000	0.000	0.000	0.000	0.000	0.000	0.000	1.868	1.614	1.592	0.331
Ni	0.000	0.000	0.000	0.000	0.000	0.000	0.000	0.000	0.000	0.097	0.346	0.446	1.683
Ca	0.000	0.000	0.000	0.000	n.a.	n.a.	0.000	0.000	0.000	0.002	0.002	n.a.	n.a.
Na	0.000	0.000	0.000	0.000	n.a.	n.a.	0.000	0.000	0.000	0.000	0.000	n.a.	n.a.
K	0.000	0.000	0.000	0.000	n.a.	n.a.	0.000	0.000	0.000	0.001	0.001	n.a.	n.a.
Σ cations	1.000	1.000	1.000	1.000	1.001	1.001	1.001	1.000	1.000	3.990	3.986	4.020	3.010

^a Phase presumed to be spinel-structured (Ni,Mg)₂SiO₄
n.a. = not analysed

indication of O-H stretching associated with hydrogen defects rather than liquid water, which typically results in a broad-band absorption in room-temperature measurements (Kronenberg 1994). Step profiles across large (ca. 200 μm) coesite crystals were conducted using a 20-μm aperture to check for zoning in hydrogen content. No significant variations were found along these profiles, indicating that the solubility of hydrogen may have reached equilibrium (although this cannot be

proven without doing reversal experiments). Spectra on crystals of different orientations, however, show small but significant differences. This effect is probably due to pleochroism in the infrared absorption, which can be a significant obstacle to quantitative determination of hydrogen contents in minerals (Rossman 1996). The orientation dependence of IR absorption in coesite is unknown. OH concentrations were determined by averaging spot analyses on several crystals of different orientations within each sample. The spectra show small changes in relative heights between the four main absorption peaks. However, the low standard deviations of the calculations (Table 1) suggest that the orientation dependence is not very strong. The evolution of the coesite spectra with pressure is shown in Fig. 4. Average concentrations (Table 1) range from 284 H/10⁶ Si (at 5 GPa) to 1415 H/10⁶ Si (at 10 GPa). The solubility at 7 GPa (729 ± 61 H/10⁶ Si) is in excellent agreement with the value of 100 ppm H₂O by weight (= 667 H/10⁶ Si) estimated by Li et al. (1997).

The spectra of stishovite (Fig. 3b) show very strong absorption at 3111 cm⁻¹, as in the study of Pawley et al. (1993), and a small peak at 3351 cm⁻¹, which was not found in their spectra. Stishovite is known to have very strong orientation dependence in IR absorption, with absorption strongest perpendicular to the *c* direction (Pawley et al. 1993). Consistent with this, unpolarized spectra of stishovite in sample no. 1109 showed widely varying peak heights. Therefore, because the orientations of the crystals could not be determined, only a

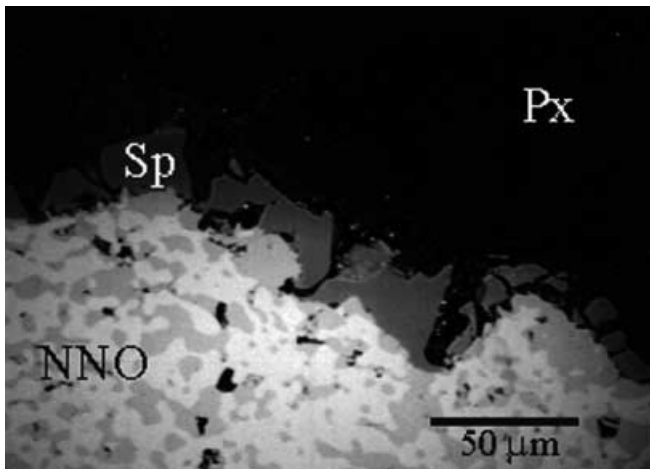
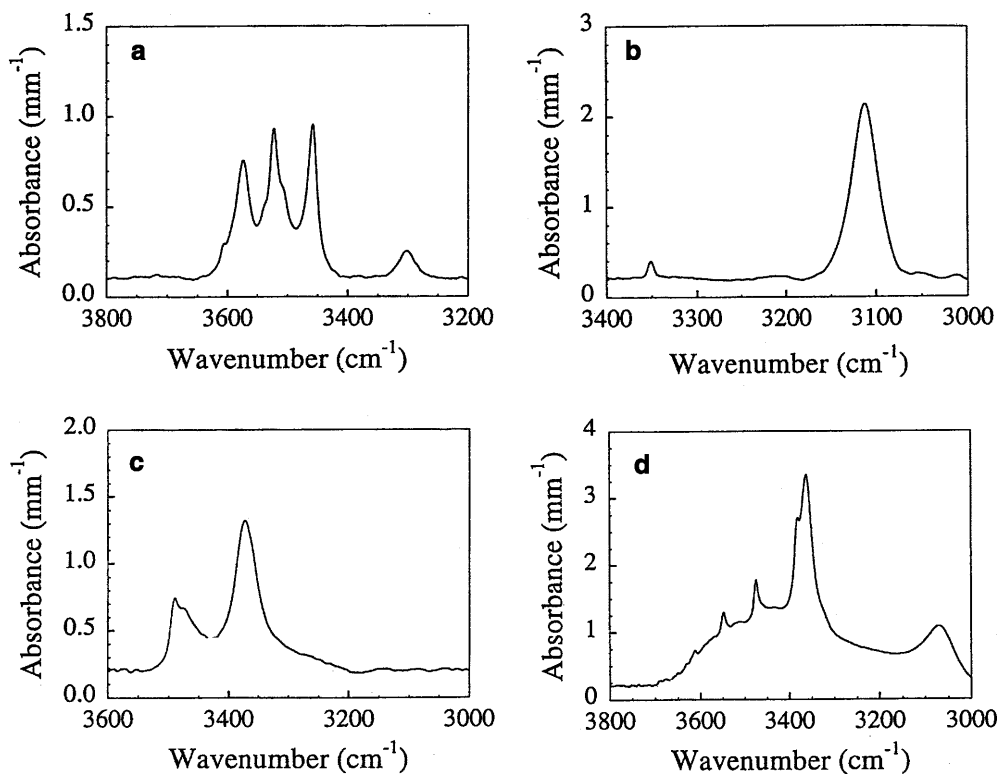


Fig. 2 BSE image of sample no. 917 showing Ni-rich pyroxene (*Px*), Ni₂SiO₄ (spinel?) reaction rim (*Sp*), and intergrowth of Ni and NiO (*NNO*)

Fig. 3a–d Typical infrared spectra of experimental products. **a** Coesite (sample no. 917), showing four main absorption peaks at 3573, 3523, 3459, and 3298 cm^{-1} . A small peak at 3606 cm^{-1} is present but not clearly visible at this scale. **b** Stishovite (sample no. 1109) **c** Ni-rich pyroxene (sample no. 917). **d** Mg-end member enstatite (sample no. S1686). All enstatite spectra collected show a broad band absorbance that may result from water on grain boundaries or in fluid inclusions



minimum estimate of the hydrogen concentration could be obtained, by integrating the absorbance of the unpolarized spectrum with the greatest peak height at 3111 cm^{-1} . Application of the Paterson (1982) calibration yielded a value of 285 H/10⁶ Si, while using the absorption coefficient of Pawley et al. (1993) gave a value of 174 H/10⁶ Si. This is somewhat higher than the value of 45 H/10⁶ Si measured for Al-free stishovite by Pawley et al. (1993), possibly reflecting the presence of small amounts of Al in stishovite (see Table 2) and/or inaccuracy of the calibration of Pawley et al. (1993).

Ni₂SiO₄ and NiO in our samples have no detectable absorbance in the 4000 to 2000 cm^{-1} region of the infrared. Ni-rich pyroxene displays two peaks at 3372 and 3490 cm^{-1} (Fig. 3c), while spectra for the Mg-end member enstatite in sample no. S1686 show sharp peaks at 3065, 3362, 3381, 3475, 3548, and 3613 cm^{-1} (Fig. 3d). These spectra are dissimilar to previously published spectra for orthopyroxenes (Skogby et al. 1990; Bell et al. 1995), presumably due to association with different trace elements in the different samples. Hydroxyl concentrations were not determined for the pyroxenes in this study because the crystals were too fine-grained to obtain spectra on clear, fluid-inclusion, and fracture-free areas.

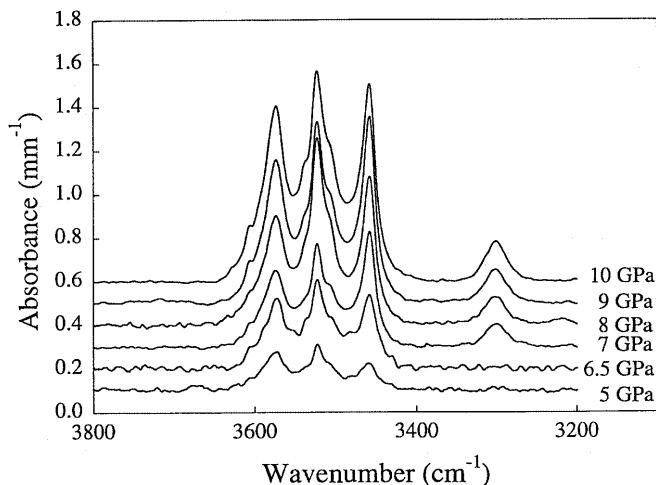


Fig. 4 Pressure dependence of infrared spectra in coesite

Discussion

Comparison to other nominally anhydrous minerals

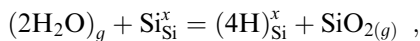
The measured concentrations indicate that the solubility of OH in coesite is comparable to that measured in synthetic quartz (Rovetta et al. 1989). The solubility of OH in coesite is also very similar to that in pyrope garnet, as measured experimentally by Lu and Keppler (1997), although a later study determined much greater OH solubilities (up to 7 GPa) for pyrope (Withers et al. 1998). In contrast, olivine (Kohlstedt et al. 1996), grossular garnet (Withers et al. 1998), and pyroxenes (Skogby et al. 1990; Smyth et al. 1991; Bell et al. 1995) can incorporate about an order of magnitude more OH than coesite at comparable pressure-temperature

conditions. Thus, although coesite could be a potentially important carrier for hydrogen in deeply subducted sialic crust, it is unlikely to play a major role in the mantle, where it is considerably less abundant.

Mechanisms and thermodynamics of incorporation of hydroxyl in coesite

The systematic increase in OH solubility with increasing pressure in the experiments implies that incorporation of hydrogen in coesite is controlled by water or hydrogen fugacity, because all the experiments (with the exception of no. S1686) were performed at similar oxygen fugacities. The experiments presented here cannot be used to address the systematic effect of differing trace element concentrations, which could be significant, as in the case of stishovite (Pawley et al. 1993). The following analysis, therefore, assumes that OH solubility is controlled by water fugacity (see, e.g., Kohlstedt et al. 1996) and that hydrogen is incorporated as point defects in the lattice of coesite.

In the absence of other impurities, the only plausible defect that could accommodate hydrogen in coesite is an Si vacancy, associated with four protons for charge balance. The formation of such $(4H)_{Si}$ defects in SiO_2 can be described by the following equation (using the notation of Kröger and Vink 1956):



with the equilibrium constant

$$K = a_{SiO_{2(g)}} a_{(4H)_{Si}^x} / (f_{H_2O}^2 a_{Si_{Si}^x}) ,$$

thus yielding a defect concentration dependent on water fugacity in the following manner:

$$C_{(4H)_{Si}^x} = \frac{1}{4} C_{OH} \propto f_{H_2O}^n .$$

Knowing this dependence, the solubility data can be fitted to the following equation (Kohlstedt et al. 1996):

$$C_{OH} = A f_{H_2O}^n \exp(-P\Delta V/RT) ,$$

with $n = 2$, in order to calculate the constants A and ΔV , where ΔV is the molar volume change of the coesite lattice due to incorporation of hydroxyl. Note that although this equation ignores enthalpy and entropy terms, they are expected to be small relative to the volume term. This equation was fitted using water fugacities calculated from the equation of state for H_2O of Pitzer and Sterner (1994), as shown in Fig. 5a, yielding values for A and ΔV of $4.38 \text{ H}/10^6 \text{ Si/GPa}$ and $20.6 \times 10^{-6} \text{ m}^3 \text{ mol}^{-1}$, respectively.

Hydrogen also can be incorporated in coesite as isolated OH defects charge balanced by substitutional impurity cations such as Al^{3+} , which may be present in our samples in sufficient abundance (Table 2). In this case, $n = 0.5$ in the above equation (Lu and Keppler 1997), and a somewhat poorer fit to the data (Fig. 5)

yields values for A and ΔV of $33.8 \text{ H}/10^6 \text{ Si/GPa}$ and $2.2 \times 10^{-6} \text{ m}^3 \text{ mol}^{-1}$, respectively.

Unfortunately, a preferred model for incorporation cannot be distinguished based on the solubility data alone and the above analysis. The existence of $(4H)_{Si}$ defects has been proposed to be responsible for incorporation of hydrogen in garnets (Aines and Rossman 1984; Lager et al. 1989) as well as quartz (McLaren et al. 1983). In the case of garnet, it is believed to be an active mechanism only at high OH contents (Rossman 1996). In quartz, in contrast, evidence for its importance at low concentrations comes from near-infrared spectra (Cordier and Doukhan 1991), electron-paramagnetic resonance (Cordier et al. 1994), and theoretical calculations (McConnell et al. 1995). At high concentrations, the $(4H)_{Si}$ defect becomes largely subsidiary to molecular water defects (Aines et al. 1984; Cordier and Doukhan 1991), which have not been described for coesite. A model of incorporation by $(4H)_{Si}$ defects therefore appears plausible for coesite. However, the alternative model of incorporation might be more consistent with the frequencies of the peaks in the IR spectra. The $(4H)_{Si}$ defect in garnet gives rise to peaks around 3600 cm^{-1} , while peaks at lower wavenumbers in quartz are

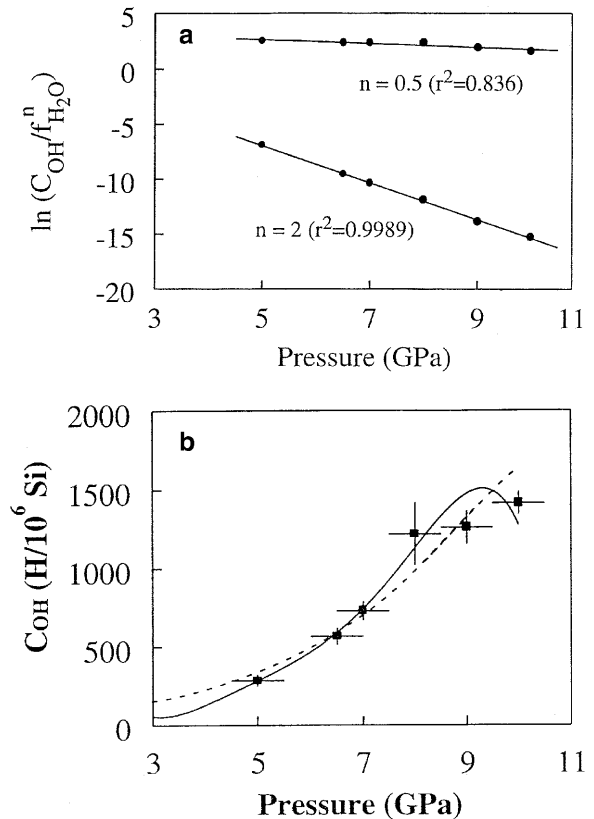


Fig. 5 **a** Semilog plot showing concentration of OH as a function of pressure and water fugacity for the two point defect models discussed in the text [isolated OH groups vs. $(4H)_{Si}$ clusters]. **b** Concentration of OH as a function of pressure. The *solid line* is the fit to the data assuming a model for incorporation as $(4H)_{Si}$ defects; the *dashed line* shows the fit assuming a model of isolated OH groups

generally associated with cation substitutions (Kronenberg 1994).

Implications for the preservation of coesite

Extrapolation of experimental kinetic data (Mosenfelder and Bohlen 1997) indicates that the transformation of coesite to quartz is rapid on geological time scales in the presence of moderate amounts of fluid (ca. 0.04 wt%). Preservation of coesite in UHP rocks has been attributed to three factors: (1) extremely rapid exhumation rates; (2) inclusion in strong host phases that inhibit reaction by exerting an overpressure on coesite (Gillet et al. 1984); and (3) lack of fluids to flux the reaction.

Geochronological data can be used to constrain the duration of exhumation of UHP rocks. In the case of the Dora Maira massif, for instance, application of several analytical techniques documents cooling from UHP metamorphic conditions to ~ 300 °C within 5–6 Ma (Gebauer et al. 1997). This implies an extremely fast exhumation rate compared to most tectonic processes. Nevertheless, in the absence of other mitigating factors, extrapolation of experimental kinetic data indicates that coesite should be completely transformed to quartz over this time scale, indeed in less than 1 Ma (Mosenfelder and Bohlen 1997). Rapid exhumation may therefore have little influence on the preservation of coesite, although it may be a factor in the preservation of transformation textures (palisade quartz) in the matrix of Dora Maira rocks (Chopin et al. 1991).

Current elastic models for coesite inclusions in garnet (e.g., Gillet et al. 1984) also fail to explain the preservation of coesite, because fracturing of the host phase by expansion of the inclusion is expected to occur at relatively high temperatures, ca. 400 °C (see Mosenfelder and Bohlen 1997). However, containment in stronger minerals such as zircon has not yet been modeled, and other complexities such as differing boundary conditions (i.e., radius of the host vs. the inclusion) and non-spherical geometry of the host or inclusion may allow for overpressuring until lower temperatures are reached. Indeed, a recent study using Raman spectroscopy to look at pressure-induced peak shifts suggests that some present-day inclusions of coesite in rocks exposed at the surface are still experiencing overpressures (Parkinson and Katayama 1999). Inclusion in strong host phases is therefore probably a major factor in the preservation of most coesite crystals.

Recent petrographic and isotopic studies have provided strong evidence for a lack of fluids attending UHP metamorphism and retrogression (Yui et al. 1995; Liou and Zhang 1996; Zhang and Liou 1997). The evidence includes preservation of intergranular coesite (Liou and Zhang 1996), the presence of which obviously cannot be explained by elastic inclusion models. The present work lends further support to the hypothesis that preservation of coesite is critically linked to a lack of fluids to flux the

reaction. Extrapolation of the experimental solubility data indicates that coesite should contain small amounts of hydrogen at typical UHP metamorphic pressures, e.g., less than 150 H/10⁶ Si at 3 GPa. Note that this estimation does not take into account probable partitioning of hydrogen between coesite and other nominally anhydrous minerals known to have much higher OH solubilities, such as omphacite (Smyth et al. 1991). Such a concentration of hydrogen is considerably less than that available to flux backreaction in the kinetic experiments of Mosenfelder and Bohlen (1997) – the equivalent of about 3000 H/10⁶ Si (primarily in the form of H₂O). Therefore, the low solubility of OH in coesite may inhibit reaction kinetics, allowing more preservation of coesite than predicted by the data of Mosenfelder and Bohlen (1997).

Moreover, FTIR investigations (Rossman and Smyth 1990; Mosenfelder 1997) have failed in all cases to detect the presence of hydrogen in natural coesite. This implies that partially preserved coesite either grows in dry environments or loses its hydrogen during ascent to the surface, perhaps during transformation to quartz. FTIR investigations on natural rocks (Mosenfelder 1997) also show that the quartz replacing coesite has varying amounts of water, implying that fluids play an important role in the transformation. In one case, from the Dora Maira massif, cathodoluminescence microscopy (H.P. Schertl pers. comm.) and FTIR show that coesite is partially replaced by microcrystalline opal (Mosenfelder 1999). This finding implies that fluid infiltration occurred at very low temperatures, presumably low enough that the kinetics of the transformation were slow even in the presence of large amounts of water.

Conclusions

The solubility of OH in coesite shows a systematic increase with pressure. The data indicate that coesite is a potentially important nominally anhydrous mineral with the capacity to incorporate amounts of hydroxyl comparable to pyrope garnet, although it is unlikely to be as important as other nominally anhydrous minerals such as olivines and pyroxenes. The existence of hydrogen defects in coesite could have important effects on its deformation behavior (Renner et al. 1996), thus influencing the rheology of silic rocks subducted to UHP conditions. However, extrapolation of the solubility data indicates that coesite is unlikely to incorporate more than ~ 150 H/10⁶ Si at typical UHP metamorphic pressures. This is also consistent with studies on natural rocks, which failed to detect the presence of hydrogen. These data, coupled with observations of natural UHP rocks, support the hypothesis that the partial preservation of coesite is not necessarily linked to rapid exhumation rates but is critically dependent on a lack of fluids to flux the reaction, and, in the vast majority of cases, containment in strong host minerals.

Acknowledgements I thank N. Bolfan-Casanova, H. Keppler, S. Mackwell, and G. Rossman for helpful discussions; S. Mackwell, J.R. Holloway, and especially D. Bell for thorough reviews of the manuscript; H.P. Schertl for sharing his results on the Dora Maira sample; G. Hermannsdörfer, H. Fischer, and H. Künfer for technical support with the experiments; H. Schulze for sample preparation; P. Asimow for financial support to do microprobe analyses at Caltech; and E. Essene for pointing out an error enabling a last-minute correction.

References

- Aines RD, Rossman GR (1984) Water in minerals? A peak in the infrared. *J Geophys Res* 89: 4059–4071
- Aines RD, Kirby SH, Rossman GR (1984) Hydrogen speciation in synthetic quartz. *Phys Chem Miner* 11: 204–212
- Bell DR, Rossman GR (1992) Water in the Earth's mantle: the role of nominally anhydrous minerals. *Science* 255: 1391–1397
- Bell DR, Ihinger PD, Rossman GR (1995) Quantitative analysis of trace OH in garnet and pyroxenes. *Am Mineral* 80: 465–474
- Chopin C, Henry C, Michard A (1991) Geology and petrology of the coesite-bearing terrain, Dora Maira massif, Western Alps. *Eur J Mineral* 3: 263–291
- Coleman RG, Wang X (1995) Overview of the geology and tectonics of UHPM. In: Coleman RG, Wang X (eds) *Ultrahigh pressure metamorphism*. Cambridge University Press, Cambridge, pp 1–32
- Cordier P, Doukhan JC (1991) Water speciation in quartz: a near-infrared study. *Am Mineral* 76: 361–369
- Cordier P, Weil JA, Howarth DF, Doukhan JC (1994) Influence of the (4H)_{Si} defect on dislocation motion in crystalline quartz. *Eur J Mineral* 6: 17–22
- Gebauer D, Schertl H-P, Brix M, Schreyer W (1997) 35-Ma-old ultrahigh-pressure metamorphism and evidence for very rapid exhumation in the Dora Maira massif, Western Alps. *Lithos* 41: 5–24
- Gillet P, Ingrin J, Chopin C (1984) Coesite in subducted continental crust: P-T history deduced from an elastic model. *Earth Planet Sci Lett* 70: 426–436
- Kohlstedt DL, Keppler H, Rubie DC (1996) Solubility of water in the α , β , and γ phases of (Mg,Fe)₂SiO₄. *Contrib Mineral Petrol* 123: 345–357
- Kröger FA, Vink HJ (1956) Relation between the concentration of imperfections in crystalline solids. In: Seitz F, Turnhall D (eds) *Solid state physics 3*. Academic Press, New York, pp 367–435
- Kronenberg AK (1994) Hydrogen speciation and chemical weakening of quartz. In: Heaney PT, Prewitt CT, Gibbs GV (eds) *Silica: physical behavior, geochemistry and materials applications*, 29. Mineral Soc Am, Washington, DC, pp 123–176
- Lager GA, Armbruster T, Rotella FJ, Rossman GR (1989) OH substitution in garnets: X-ray and neutron diffraction, infrared, and geometric-modeling studies. *Am Mineral* 74: 840–851
- Li W, Lu R, Yang H, Prewitt CT, Fei Y (1997) Hydrogen in synthetic coesite crystals. *EOS* 78: 736
- Liou JG, Zhang RY (1996) Occurrences of intergranular coesite in ultrahigh-P rocks from the Sulu region, eastern China: implications for lack of fluid during exhumation. *Am Mineral* 81: 1217–1221
- Lu R, Keppler H (1997) Water solubility in pyrope to 100 kbar. *Contrib Mineral Petrol* 129: 35–42
- McConnell JDC, Lin JS, Heine V (1995) The solubility of [4H]Si defects in α -quartz and their role in the formation of molecular water and related weakening on heating. *Phys Chem Miner* 22: 357–366
- McLaren AC, Cook RF, Hyde ST, Tobin RC (1983) The mechanisms of the formation and growth of water bubbles and associated dislocation loops in synthetic quartz. *Phys Chem Miner* 9: 79–94
- Mosenfelder JL (1997) Fluids, the preservation of coesite, and the exhumation of UHP metamorphic rocks. *Terra Abstr* 9: 20–21
- Mosenfelder JL (1999) Water solubility in coesite: implications for the preservation of coesite in ultra-high pressure rocks. *EOS* 80: 986
- Mosenfelder JL, Bohlen SR (1997) Kinetics of the coesite to quartz transformation. *Earth Planet Sci Lett* 153: 133–147
- Parkinson CD, Katayama I (1999) Present-day ultrahigh-pressure conditions of coesite inclusions in zircon and garnet: evidence from laser Raman spectroscopy. *Geology* 27: 979–982
- Paterson M (1982) The determination of hydroxyl by infrared absorption in quartz, silicate glasses and similar materials. *Bull Mineral* 105: 20–29
- Paterson M (1989) The interaction of water with quartz and its influence in dislocation flow – an overview. In: Karato S-I, Toriumi M (eds) *Rheology of solids and of the Earth*. Oxford University Press, Oxford, pp 107–142
- Pawley AR, McMillan PF, Holloway JR (1993) Hydrogen in stishovite, with implications for mantle water content. *Science* 261: 1024–1026
- Pitzer KS, Sterner SM (1994) Equations of state valid continuously from zero to extreme pressures for H₂O and CO₂. *J Chem Phys* 101: 3111–3116
- Renner J, Rummel F, Stoeckhert B (1996) Experimental deformation of synthetic coesite aggregates. *EOS* 77: 717
- Rossman GR (1996) Studies of OH in nominally anhydrous minerals. *Phys Chem Miner* 23: 299–304
- Rossman GR, Smyth JR (1990) Hydroxyl contents of accessory minerals in mantle eclogites and related rocks. *Am Mineral* 75: 775–780
- Rovetta MR, Blacic JD, Hervig RL, Holloway JR (1989) An experimental study of hydroxyl in quartz using infrared spectroscopy and ion microprobe techniques. *J Geophys Res* 94: 5840–5850
- Rubie DC (1999) Characterising the sample environment in multianvil high-pressure experiments. *Phase Trans* 68: 431–451
- Rubie DC, Tsuchida Y, Yagi T, Utsumi W, Kikegawa T, Shimomura O, Brearley AJ (1990) An in situ X ray diffraction study of the kinetics of the Ni₂SiO₄ olivine-spinel transformation. *J Geophys Res* 95: 15,829–15,844
- Rubie DC, Ross CR, Carroll MR, Elphick SC (1993) Oxygen self-diffusion in Na₂Si₄O₉ liquid up to 10 GPa and estimation of high-pressure melt viscosities. *Am Mineral* 78: 574–582
- Skogby H, Bell DR, Rossman GR (1990) Hydroxide in pyroxene: variations in the natural environment. *Am Mineral* 75: 764–774
- Smyth JR, Bell DR, Rossman GR (1991) Incorporation of hydroxyl in upper-mantle clinopyroxenes. *Nature* 351: 732–735
- Withers AC, Wood BJ, Carroll MR (1998) The OH content of pyrope at high pressure. *Chem Geol* 147: 161–171
- Yui T-F, Rumble III D, Lo C-H (1995) Unusually low $\delta^{18}\text{O}$ ultrahigh-pressure metamorphic rocks from the Sulu Terrain, eastern China. *Geochim Cosmochim Acta* 59: 2859–2864
- Zhang RY, Liou JG (1997) Partial transformation of gabbro to coesite-bearing eclogite from Yangkou, the Sulu terrane, East China. *J Metam Geol* 15: 183–202
- Zhang J, Li B, Utsumi W, Liebermann RC (1996) In situ X-ray observations of the coesite-stishovite transition: reversed phase boundary and kinetics. *Phys Chem Miner* 23: 1–10